Electron-paramagnetic-resonance measurements on the divacancy defect center $R4/W6$ in diamond

D. J. Twitchen, M. E. Newton,* and J. M. Baker
Department of Physics, University of Oxford, Clarendon Laboratory, Parks Road, Oxford OX1 3PU, United Kingdom

T. R. Anthony
General Electric Company, Corporate Research and Development, Building K1, Room IC30, Schenectady, New York 12301

W. F. Banholzer
General Electric Lighting, 1975 Noble Road, Nela Park, Cleveland, Ohio 44112-6300
(Received 19 January 1999)

Electron-paramagnetic-resonance (EPR) studies in radiation damaged diamond enriched to 5% ^{13}C have resulted in the identification of the nearest-neighbor divacancy center. It is the isotopic enrichment, and consequent observation of ^{13}C hyperfine lines, that has permitted the structure to be determined more than 30 years after the discovery of the center, known as $R4$ or $W6$. The center is produced by annealing radiation damaged diamonds to temperatures at which the vacancy is mobile (above about 900 K), and in pure diamond it is the dominant vacancy related product of irradiation and 900 K annealing. The divacancy anneals out upon prolonged annealing to temperatures above about 1100 K. Low-temperature EPR measurements determine the absolute sign of the largest principal value of the $\underline{\mathbf{D}}$ matrix, D_3 to be negative; and measurements at temperatures between 4.2 and 300 K indicate that the $\underline{\mathbf{D}}$ matrix is temperature dependent in this interval. The center has C_{2h} symmetry at low temperatures (30 K), and appears to change to axial symmetry about $\langle 111 \rangle$ at high temperatures (>400 K). Analysis of the ^{13}C hyperfine-coupling data using a simple molecular-orbital model shows that at low temperature the unpaired electron probability density is primarily located on four equivalent carbon atoms that are not in the $\{110\}$ plane of reflection symmetry containing the two vacancies. These four carbon atoms show an outward relaxation around the divacancy. The low-temperature symmetry and localization of the unpaired electron probability density is surprising, the former in the light of theoretical predictions of a $^3A_{2g}$ ground state in the undistorted D_{3d} symmetry and the latter in comparison with divacancies in silicon. A simple defect molecule calculation suggests that the divacancy has a ^3B_u ground state at low temperatures with C_{2h} symmetry. The large linewidth leaves it unclear whether the symmetry changes at high temperatures to D_{3d}. The broadening of the EPR linewidth with increasing temperature does not originate from thermally activated reorientation between sites with C_{2h} symmetry. It appears to be due to rapid spin-lattice relaxation (via the Orbach mechanism) at temperatures above 50 K, and simple analysis suggests that there is an excited state 20(1) meV above the ground state. [S0163-1829(99)04620-2]

I. INTRODUCTION

Recent advances in diamond synthesis, and more importantly the quality and size of the manufactured diamond, are stimulating interest in exploiting diamond in applications where its remarkable physical properties enable technological breakthroughs. Low-dielectric loss diamond windows for high power gyrotrons, diamond visible blind ultraviolet photodetectors, and ionizing particle detectors are some of the most promising recent applications. The fundamental physical properties (high-thermal conductivity, optical transparency, mechanical strength, etc.) that make diamond an attractive optical/electronic engineering material are very sensitivite to impurities and defects. Successful exploitation in applications where diamond is likely to suffer radiation damage demand a thorough understanding of radiation damage defect formation, migration, aggregation, and annealing. In this paper, we present electron-paramagnetic-resonance (EPR) measurements on a defect in diamond that is produced by electron irradiation and annealing to 900-1000 K. The results presented in this paper show that this center is the nearest-neighbor divacancy in the neutral charge state.

This paper will be set out as follows: previous work on the vacancy and divacancy in diamond and silicon will be reviewed in the remainder of the introduction; experimental details given in Sec. II; our new measurements presented in Sec. III, their significance discussed in Sec. IV, and Sec. V describes how the evidence leads to a model for the center. Finally our conclusions are presented in Sec. VI.

A. The isolated vacancy in diamond

The lattice vacancy in diamond, one of the primary products of radiation damage, has been extensively studied. Experiment and theory for the neutral and negatively charged vacancies are in good accord. The early theoretical defect molecule calculations of Coulson and Kearsley[1] for the diamond lattice vacancy were remarkably successful because they recognized that there are several possible ground states for the vacancy, and as a consequence electron-electron correlation effects are important. In the defect molecule calculation they assumed that the electronic properties are prima-

rily determined by the electrons in the dangling orbitals surrounding the vacancy. The T_d-point group requires that these orbitals transform as a_1 and t_2. For the neutral vacancy these orbitals are filled with four electrons in the configurations $a_1^2t_2^2$, $a_1^1t_2^3$, or t_2^4. The configuration $a_1^2t_2^2$ gives rise to the many-electron states $^1A_1$, ^1E, $^3T_1$, and $^1T_2$. Optical absorption measurements on V^0 show that its characteristic zero-phonon absorption line (labeled GR1) at 1.673 eV originates from a ^1E to $^1T_2$ transition within the $a_1^2t_2^2$ configuration and that the ground state is ^1E, as predicted by Coulson and Kearsley.[1] This degenerate ground state suffers a dynamic Jahn-Teller distortion that splits it into an E (ground) and A state (8 meV higher).[2] For the negatively charged vacancy, the a_1 and t_2 states are filled with five electrons. The configuration $a_1^2t_2^3$ gives rise to the many electron states $^4A_2$, ^2E, $^4T_1$, $^2T_1$, and $^2T_2$, of which $^4A_2$ is predicted to be the ground state, this has indeed been confirmed by EPR measurements.[3] EPR measurements on the $^4A_2$ ground state of the negative vacancy, and the $^5A_2$ excited state (populated by optical excitation) of the neutral vacancy show that in both charge states the unpaired electron population is predominately localized in the carbon dangling orbitals and that the symmetry remains as T_d.[3,4]

Lattice relaxation at the vacancy in diamond has been investigated using a Car-Parrinello molecular-dynamics calculation,[5] and a cluster model (local-density-pseudopotential theory).[6] The former predicted outward displacement of the nearest neighbors of V^0 by 0.011 nm and the latter an outward displacement of 0.02 nm in both the neutral and negative charge states. Using the hybridization ratio determined from ^{13}C hyperfine coupling parameters,[3,4] we estimate that the nearest neighbors relax away from the vacancy by $\sim$0.02 nm in both the neutral and negative charge states. Theory and experiment appear to be in accord, predicting an outward displacement of the nearest neighbors by $\sim$10% of the normal C-C bond length and little displacement for the next-nearest neighbors.

The activation energy for neutral vacancy migration has been determined to be 2.3(1) eV, and it was found that the negatively charged vacancy converts to the neutral charge state before migrating.[7] The high migration energy implies that high-temperature annealing ($\geqslant$900 K) is required for divacancy formation by aggregation. Mobile vacancies are readily trapped by nitrogen centers and at significant nitrogen concentrations the probability of divacancy formation is dramatically reduced.[7]

B. Previous work on the divacancy in diamond

In diamond with impurity content less than 0.1 parts per million carbon atoms (ppm.) (labeled type IIa) most of the EPR and optical centers created by radiation damage and annealing fall roughly into two categories: those existing below 900 K and those developing above 1000 K. Only one EPR center, labeled $R4$ or $W6$ in the literature (from now on referred to as $R4/W6$), is prominent in the intermediate temperature interval.[8] EPR measurements at 80 K showed that the $R4/W6$ center has $S=1$ and C_{2h} symmetry. It has recently been shown that the concentration of $R4/W6$ centers correlates with the optical-absorption band TH5 (2.3–2.8 eV).[8] Early work by Clark *et al.*[9] suggested that TH5 was formed from two vacancies. Large concentrations of $R4/W6$ can be produced in type IIa diamonds, but only low concentrations are ever produced in type Ia/Ib diamonds where nitrogen centers provide competing traps for mobile vacancies. When the nitrogen concentration greatly exceeds the vacancy concentration $R4/W6$ and TH5 are not observed after annealing to temperatures at which the vacancy is mobile. The data outlined above led Lea-Wilson *et al.* to speculate that $R4/W6$ was the nearest-neighbor divacancy in the neutral charge state ($[V\text{-}V]^0$).[8] We present data that shows that this proposal is correct, and provide detailed information on the structure of the defect.

Two possible divacancy structures have attracted theoretical study, $[V\text{-}V]$ and the [110] divacancy with the structure $[V\text{-}C\text{-}V]$. Coulson and Larkins investigated the electronic structure of $[V\text{-}V]^0$ using the defect-molecule approach previously applied to the isolated vacancy.[10] The nearest-neighbor undistorted divacancy has D_{3d} symmetry so that the single-electron molecular orbitals formed from the appropriate linear combinations of the six dangling orbitals must belong to the irreducible representations a_{1g}, a_{2u}, e_u, and e_g. For the neutral divacancy, these orbitals are filled with six electrons. Application of Hunds rules would lead one to predict that the ground state was $^7A_{2u}$ from the one electron configuration $a_{1g}a_{2u}e_u^2e_g^2$. However, the promotion of electrons from the a_{1g} and a_{2u} states is energetically expensive, and Coulson and Larkins predicted that the ground state was $^3A_{2g}$ (arising from the one electron configuration $a_{1g}^2a_{2u}^2e_u^2$). This orbital singlet ground state would not show any Jahn-Teller effect. Coulson and Larkins calculation suggested that it was unlikely that the Jahn-Teller effect was sufficiently large to split an excited state orbital doublet and shift one of its components below the $^3A_{2g}$ level, so no Jahn-Teller distortion of the center was expected. The predicted ground state is paramagnetic ($S=1$), however the D_{3d} symmetry is not consistent with the C_{2h} symmetry observed for $R4/W6$.

The next-nearest, split or $\langle 110\rangle$ divacancy ($[V\text{-}C\text{-}V]$) has C_{2v} symmetry. We know of no detailed electronic structure calculations for this defect in diamond. A recent molecular dynamic calculation suggests that the formation energy for this structure is lower than for the $\langle 111\rangle$ divacancy.[11] This finding is at odds with similar calculations for the divacancy in silicon and not supported by the experimental evidence.

C. The vacancy and divacancy in silicon

Our understanding of vacancies in silicon is primarily based on the paramagnetic resonance work of Watkins and coworkers.[12] The positively and negatively charged vacancies were both found to have spin-one-half ground states and the neutral vacancy was found to be diamagnetic. The V^+ and V^0 centers were shown to have D_{2d} symmetry and V^- to have C_{2v} symmetry. The electronic structure of the different charge states of the isolated vacancy were modeled using a one-electron defect molecule (concentrating on the dangling bonds). It was assumed that the electrons pair off whenever possible and the Jahn-Teller effect dominates over any corrections to the one electron model. The simple one-electron approach works surprisingly well in view of the theoretical prediction that the many-electron effects should be more important than the Jahn-Teller effect. For $V^+(a_1^2t_2)$ there is

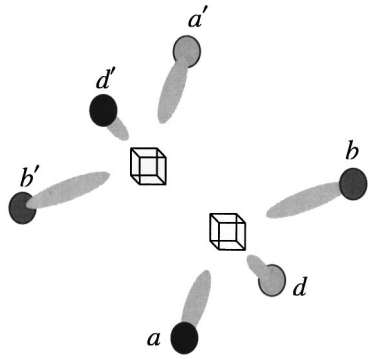

FIG. 1. Schematic diagram of the ⟨111⟩ divacancy center in diamond or silicon. The labeling of the dangling orbitals/atoms is used throughout the paper and is consistent with the notation used by Watkins and Corbett [Phys. Rev. **138**, A543 (1965)].

only a single electron in the t_2 state so that only the Jahn-Teller splitting need be considered (tetragonal distortion to D_{2d} symmetry). For $V^0(a_1^2t_2^2)$ calculations predict that the Jahn-Teller effect (tetragonal distortion to D_{2d} symmetry) dominates over the correction arising from including electron correlation effects. However, for $V^-(a_1^2t_2^3)$ the situation is complicated (mixed tetragonal and trigonal distortions in the one-electron model are consistent with the experimental data) and only recently has there been progress to a better understanding of the importance of many-electron effects and the Jahn-Teller interaction.[13]

Vacancies in silicon are rapid diffusers, for V^0 the migration activation energy is 0.45 eV.[12] Vacancies in silicon are know to form pairs with acceptors (B, Al, Ga), donors (P, As, Sb), and other impurities (C, Ge, etc.). They also interact with each other to form the ⟨111⟩ divacancy, shown schematically in Fig. 1. Structure calculations suggest that the split or ⟨110⟩ divacancy has a higher formation energy than the nearest-neighbor divacancy.[14] The positively and negatively charged ⟨111⟩ divacancy were identified by EPR and found to have C_{2h} symmetry.[15] In both charge states the highest occupied level has unpaired electron probability density in the mirror plane of C_{2h} symmetry. Watkins and Corbett proposed that the four out of plane atoms surrounding the divacancy pull together to form a bent pair bond.[15] The remaining electrons are then accommodated in the extended orbital formed between the two nearest neighbor in plane silicon atoms. In terms of the one-electron defect molecule model the undistorted defect (D_{3d} symmetry) has the configuration $a_{1g}^2a_{2u}^2e_u^m$ where $m=1$ or 3 for V_2^+ or V_2^-, respectively. Because of the degeneracy associated with the partially filled e_u orbitals, a Jahn-Teller distortion takes place, lowering the symmetry to C_{2h}. These authors concluded that the Jahn-Teller distortion is sufficiently large that the a_g level, which splits off from the upper e_g level, is lowered to a position below the rising a_u level. Under this scheme for V_2^+ the one-electron energy level filling is either $a_g^2b_u^2a_g^1$ or $a_g^2b_u^2b_u^1$ and for V_2^- $a_g^2b_u^2a_g^2b_u^1$ or $a_g^2b_u^2b_u^2a_g^1$ (the ordering of a_g and b_u is uncertain).

The nature of the symmetry lowering distortion has been the topic of recent debate. Saito and Oshiyama's calculation[16] suggests that for V_2^+ there is a weak-pairing distortion (giving rise to electronic configuration $a_g^2b_u^2b_u^1$), but for V_2^- the distortion is not a pairing distortion but *resonant bonding* (giving rise to electronic configuration $a_g^2b_u^2a_u^2b_u^1$) with the distance between atoms a and d (l_{ad}) longer than l_{ab} and l_{bd}, which are equal (for notation see Fig. 1).[17,18]

II. EXPERIMENTAL

The single-crystal diamond sample used for the studies presented here was grown at high temperatures and pressure by the temperature gradient method, from diamond powder produced by chemical-vapor deposition. The diamond powder used for the growth of the sample was isotopically enriched with 5% ^{13}C. Raman measurements on the sample produced showed that the abundance of ^{13}C was 4.8(5)%. The sample was mounted in an indium/gallium eutectic on a water cooled copper block and irradiated using 1.9 MeV electrons at a beam current of 16 μA to a dose of 6.5×10^{17} electrons cm^{-2}.

Most of the EPR measurements were made using the *Q*-band (nominally 35 GHz) spectrometer described previously by Twitchen *et al.*[19] The increased sensitivity, and the ability to collect spectra in dispersion mode (where the effects due to saturation are reduced), allowed the ^{13}C hyperfine lines in the sample to be observed and studied at 33 K. For the *Q*-band EPR measurements sample temperatures between 4 and 300 K were achieved using an Oxford Instruments continuous flow cryostat (CF200). In order to produce temperatures down to 1.5 K for the low-temperature EPR measurements (Sec. III C), the sample was cooled using a Clarendon-built immersion cryostat. This was filled with liquid helium and the temperature was reduced by pumping on the helium with a large displacement rotary pump. *X*-band (nominally 9.5 GHz) EPR measurements at temperatures between 4 and 300 K were made with a Bruker ER200D EPR spectrometer, equipped with a TE_{104} cavity and an ESR900 continuous flow cryostat. Concentration measurements were made by comparing doubly integrated first harmonic EPR absorption spectra with those of a well-calibrated reference sample—a single growth sector HTHP synthetic Ib diamond, which contained 242(20) ppm of the paramagnetic single substitutional nitrogen defect (P1).[20]

Optical-absorption measurements in the visible and UV regions of the spectrum were made with a Perkin Elmer Lambda 9 spectrophotometer, with the sample mounted in a continuous flow cryostat. The temperature of the sample could be varied between 8 and 300 K. The neutral vacancy concentration (number per cm^3) was determined by dividing the integrated absorption (in units meV cm^{-1}) of the GR1 zero phonon line by $1.2(3)\times10^{-16}$. This factor has been determined from a series of measurements described elsewhere.[21] Infrared-absorption measurements were made at room temperature using a Perkin-Elmer 1710 infrared Fourier-transform spectrometer.

III. RESULTS

A. Optical absorption, annealing, and defect-concentration measurements

In the sample used in this work the infrared absorption in the one phonon region (energy less than 1332 cm^{-1}) was

immeasurably small. The concentration of neutral single substitutional nitrogen in the sample is below the detection limit of infrared absorption (~ 5ppm). No EPR centers were detected in the as grown sample. As well as the characteristic multiphonon diamond absorption, weak absorption maxima at 2455, 2801, and 2922 cm^{-1} (0.305, 0.348, and 0.363 eV) were seen before irradiation. These are electronic transitions associated with the neutral substitutional boron acceptor. Collins and Williams[22] showed that the neutral acceptor concentration may be estimated from the integrated absorption of the 0.348 eV band. Using their data we estimate that the neutral boron concentration before irradiation was $\sim 10^{16}$ cm^{-3} ($\sim$0.1 ppm). This measurement sampled about 50% of the specimen and should be taken as a mean concentration. After irradiation the absorption from the neutral boron centers had completely disappeared. On annealing to 1000 K the boron absorption did not recover.

Before irradiation no absorption was detected in the visible or ultraviolet spectrum below the indirect band-gap energy of 5.5 eV. Using the standard notation for different types of diamond this specimen would be classified IIa/IIb(weak).

After irradiation at room temperature with 1.9 MeV electrons to a dose of 6.5×10^{17} cm^{-2}, the visible/UV absorption spectra measured at 80 K showed strong absorption from the neutral vacancy (GR1) with the characteristic zero phonon line (ZPL) at 1.673(1) eV. At 10 K, the full width at half height of the 1.673 eV ZPL was 1.3(1) meV. After irradiation, but before any anneal, the concentration of V^0 was $(8\pm 2)\times 10^{16}$ cm^{-3}, the $R4/W6$ EPR center was not observed and no absorption from the TH5 absorption band was detected. The concentration of V^- was two orders of magnitude lower than the V^0 concentration and was not monitored during anneals.

Initially the sample was annealed to 600 K for 2 h. After this anneal, the V^0 concentration was reduced by 17(3)% to $(6.6\pm 2)\times 10^{16}$ cm^{-3}. Changes at this temperature correspond to the loss of vacancies through interstitial migration and annihilation with vacancies, and not vacancy migration.[7] Further annealing at 600 K had no effect on the V^0 concentration, the $R4/W6$ EPR center was not observed and no absorption from the TH5 absorption band was detected.

On annealing the sample to 1000 K for one hour, and remeasuring the neutral vacancy concentration, it was found that the concentration of V^0 had been reduced further by $(1.5\pm 0.4)\times 10^{16}$ cm^{-3}. The $R4/W6$ EPR center and the TH5 optical-absorption band were both observed after this anneal. The measured concentration of $R4/W6$ was $(0.6\pm 0.2)\times 10^{16}$ cm^{-3}. Hence, within errors this result is consistent with $R4/W6$ being formed from two V^0 centers and under these annealing conditions the formation of $R4/W6$ is the dominant product of V^0 migration and aggregation.

B. EPR spectra at 33K

After annealing to 1000 K for 1 h, $R4/W6$ was the dominant EPR center detected at 33 K. All spectra were taken at 33 K to avoid linewidth broadening and with the spectrometer tuned to dispersion to avoid excessive microwave power saturation. The linewidth with the Zeeman field along the $\langle 111\rangle$ direction was 0.13(1) mT at 33 K. The linewidth did not change between 33 and 4 K.

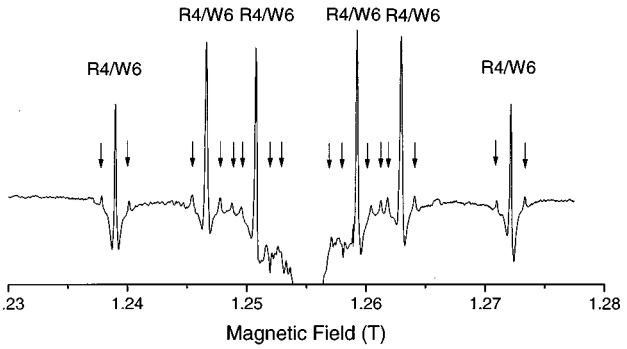

FIG. 2. First harmonic EPR spectrum collected in dispersion mode at Q band with the Zeeman field oriented along a $\langle 111\rangle$ crystallographic axis. The EPR transitions from the $R4/W6$ EPR center with no ^{13}C near neighbors are labeled. The ^{13}C hyperfine satellites labeled x arise from a set of four equivalent carbon atoms are indicated by arrows. The data were recorded at a temperature of 33 K, the microwave frequency approximately 35.0 GHz and the microwave power incident on the TE_{011} cavity was about 0.2 mW.

Figure 2 shows the first harmonic EPR spectrum (collected in dispersion) of $R4/W6$ with the Zeeman field oriented along a $\langle 111\rangle$ crystallographic axis. The lines labeled $R4/W6$ arise from defects with only ^{12}C nearest neighbors, which have no resolved hyperfine structure. The absorption seen in the $g=2.00$ region of the spectrum in Fig. 2 arises from other EPR centers created by irradiation and annealing. Two further sets of lines associated with $R4/W6$ were also identified (x and y). The x satellites are indicated by arrows in Fig. 2. The second set of satellites (y) are difficult to observe in Fig. 2 because the splitting about the central transition is very small. The satellites (x and y) arise from defects with a ^{13}C atom in a specific (nearest-neighbor) position. The probability of finding a $R4/W6$ center with ^{13}C atoms in two or more near-neighbor positions is so low that the satellites would be too weak to observe in Fig. 2. As a consequence of the broadening of the $R4/W6$ lines as the temperature is raised, it was not possible to observe any ^{13}C hyperfine satellites above ~ 50 K.

C. Low-temperature EPR measurements

Q-band EPR measurements were made on the $R4/W6$ center at 2 K. Care was taken to eliminate saturation effects, by running at very low-incident microwave powers, and to collect the spectrum in dispersion. The temperature was measured, in the absence of the Zeeman field, using a silicon diode positioned just outside the EPR cavity. The ratio of intensities of the $M_S=+1\Rightarrow M_S=0$ and $M_S=0\Rightarrow M_S=-1$ transitions measured at 2.0(1) K when the Zeeman field was oriented along the principal direction of the $\underline{\mathbf{D}}$ matrix confirmed both that D_3 is negative and that $S=1$ for the ground state of this center.

D. Temperature variation of the EPR spectra

During the initial study, when finding the optimum conditions for observing $R4/W6$, a temperature variation of the $\underline{\mathbf{D}}$ matrix and EPR linewidth was observed. The first har-

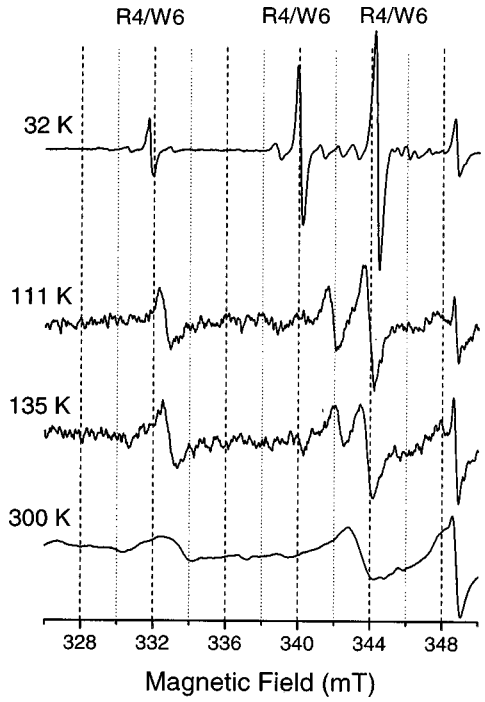

FIG. 3. First harmonic EPR spectrum collected in absorption, with the Zeeman field oriented along a ⟨111⟩ crystallographic axis. The microwave frequency was approximately 9.5 GHz. Note the change in linewidth and position of the EPR lines as a function of temperature. Extensive signal averaging (200 averages over 24 h) was required to produce the 300 K EPR spectrum.

monic EPR spectrum taken at 9.5 GHz with the Zeeman field oriented along the ⟨111⟩ crystallographic axis is shown in Fig. 3. The EPR transitions from the $R4/W6$ EPR center with no ^{13}C near-neighbors are labeled. There is a marked change of the EPR linewidth and position of the EPR lines as a function of temperature. At 33 K the spectrum shows that the defect has C_{2h} symmetry, and at 300 K the spectrum indicates axial symmetry about ⟨111⟩ which is consistent, within the linewidth, of D_{3d} symmetry.

IV. ANALYSIS OF THE DATA

A. Interpretation of the EPR spectra at 33 K

The angular variation of the EPR transitions measured at 33 K from the $R4/W6$ centers with only ^{12}C near neighbors, confirmed Lea-Wilson *et al.*[8] finding that the defect has C_{2h} symmetry, i.e., the defect has a {110} symmetry plane (containing two of the principal axes of the $\underline{\mathbf{g}}$ and $\underline{\mathbf{D}}$ matrices) and there are 12 possible symmetry related sites. The $\underline{\mathbf{g}}$ and $\underline{\mathbf{D}}$ matrices of the $R4/W6$ center were determined from fitting the experimental positions of the EPR transitions (measured at 33 K) to Eq. (1):

$$\mathcal{H}=\mu_B \mathbf{S}\cdot\underline{\mathbf{g}}\cdot\mathbf{B}+\mathbf{S}\cdot\underline{\mathbf{D}}\cdot\mathbf{S}. \quad (1)$$

The best fit values for the $\underline{\mathbf{g}}$- and $\underline{\mathbf{D}}$-matrix parameters are given in Table I. In the final fit, the $\underline{\mathbf{g}}$ and $\underline{\mathbf{D}}$ matrices were constrained to have a principal component along the ⟨110⟩ direction perpendicular to the plane of reflection symmetry, as this did not reduce the quality of the fit. In Fig. 4, the dashed lines show the angular dependence of the EPR transitions calcualted using the parameters in Table I.

TABLE I. The principal components of the $\underline{\mathbf{g}}$ and $\underline{\mathbf{D}}$ matrices of the $R4/W6$ defect center determined from experimental data collected at Q band (nominally 35 GHz) at 33 K. The angles $[\theta,\phi]$ refer to spherical coordinates expressed in the cubic axis system, and the data are presented for the site with the [110] plane of mirror symmetry. In the final fit g_1 and D_1 were constrained to be along [90°,315°]. Removing this constraint did not improve the quality of the fit.

$R4/W6$ EPR center	
$\underline{\mathbf{g}}$ matrix	$\underline{\mathbf{D}}$ (MHz)
$g_1=2.0022(1)$ [90°,315°]	$D_1=+103(2)$ [90°,315°]
$g_2=2.0026(1)$ [141(2)°,45°]	$D_2=+206(2)$ [144.2(5)°,45°]
$g_3=2.0013(2)$ [51(2)°,45°]	$D_3=-310(2)$ [54.2(5)°,45°]

The intensity of the ^{13}C satellites relative to the central transition allows the number of equivalent carbon atom positions to be determined. If satellites arise from a carbon atom in one of n equivalent positions, then, using the abundance of ^{13}C in the sample [4.8(5)%], the calculated relative intensity is 10(1)%, 16(2)%, and 20(2)% for $n=2$, 3, and 4, respectively. The intensities of transitions from different symmetry related sites in Fig. 2 do not match the predicted

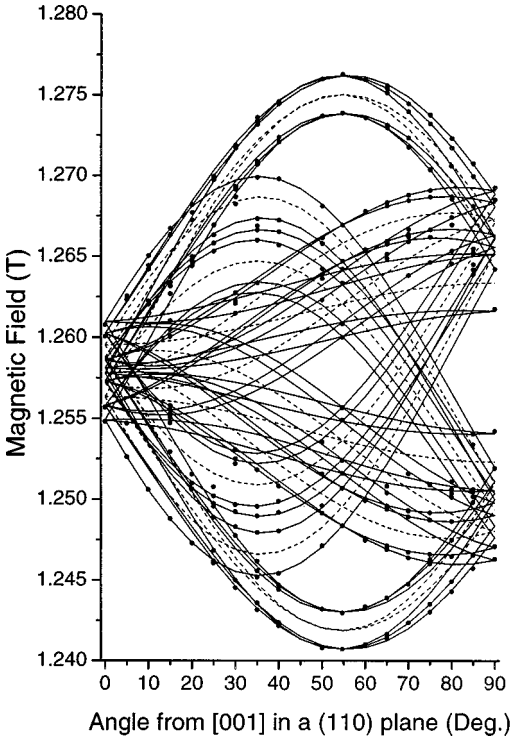

FIG. 4. Angular dependence of the principal ^{13}C hyperfine interaction of the $R4/W6$ center for rotation about the [110] axis, with θ measured from [001]. The dots are experimental line positions, measured at microwave frequencies around 35 GHz. The solid and dashed curves are calculated at 35 GHz using the $\underline{\mathbf{g}}$ and $\underline{\mathbf{D}}$ and $\underline{\mathbf{A}}$ matrices determined from fitting the experimental data. The dashed line shows the corresponding angular dependence of the EPR transitions from $R4/W6$ centers with no ^{13}C near neighbors. All experimental data were taken at ~33 K.

TABLE II. ^{13}C hyperfine constants, and the wave-function parameters calculated from them, for the $R4/W6$ center. The direction of $A_\parallel$ is given by $[\theta,\phi]$ and is appropriate for the defect site with D_1 parallel to $[90.0°,315.0°]$. Derived from experimental data collected at 33 K. See text for further details.

Satellite/	Number of equivalent C atoms	$A_\parallel$ (MHz)	$A_\perp$ (MHz)	$[\theta,\phi]$	A_S (MHz)	A_p (MHz)	η^2	λ^2
x	4	114(1)	56(1)	$[\pm 55(2)°,315.0(5)°]$	75	19	0.20	9
y	2	13(2)	13(2)		13	0	0.01	0

relative intensities as a consequence of microwave power saturation. However, the intensity of the ^{13}C satellites relative to the central transition arising from the same set of equivalent sites was found to be insensitive to microwave power saturation. The relative intensity of the x satellites to the appropriate central transition (Fig. 2) is only consistent with there being four equivalent positions for that neighbor. The intensity of the y satellites is consistent with two equivalent positions.

The angular variation (Fig. 4) and relative intensities of the x satellites is reproduced by assuming that the ^{13}C hyperfine interaction is axially symmetric and that there are four possible orientations of the principal component, $A_\parallel$, along $\langle 111\rangle$ directions not found in the $\{110\}$ mirror symmetry plane of the defect. We note that for unpaired electron probability density in a dangling orbital pointing into a lattice vacancy we expect an axially symmetric hyperfine interaction with $A_\parallel$ along the $\langle 111\rangle$ direction of the orbital (see studies on V^0 and V^-).[3,4] No other selection of symmetry related directions for $A_\parallel$ was consistent with the experimental data.

The hyperfine matrix for the x satellites was determined by least squares fitting the experimental data (84 experimental points) to the spin Hamiltonian given in Eq. (2) with I=1/2 and $g_N=1.40482$ for ^{13}C. The hyperfine interaction was constrained to have axial symmetric with $A_\parallel$ oriented along one of the out of plane $\langle 111\rangle$ directions.

$$\mathcal{H}=\mu_B \mathbf{S}\cdot\underline{\mathbf{g}}\cdot\mathbf{B}+\mathbf{S}\cdot\underline{\mathbf{D}}\cdot\mathbf{S}+\mathbf{S}\cdot\underline{\mathbf{A}}\cdot\mathbf{I}-\mu_N g_N \mathbf{I}\cdot\mathbf{B}. \qquad (2)$$

The magnitude of the $\underline{\mathbf{D}}$ matrix was sufficiently large that second-order corrections to the satellite positions cannot be ignored and the full Hamiltonian has to be used. If all the interaction matrices were collinear, then this correction would be of order $(D/g\mu_B B)^2 A$, but they are not and the correction is several times larger. The fit obtained using an exact solution of the full spin Hamiltonian was excellent, the root mean squared deviation (RMSD) error in the positions of the satellites was less than 1 MHz. The hyperfine parameters determined for the (x) satellites are given in Table II. Figure 4 shows the calculated angular variation (solid curves) for the x satellites, determined using Eq. 2 and the experimentally determined parameters. The experimental data points used in the fitting of the hyperfine parameters are shown with dots. (The dashed line shows the angular variation of the $R4/W6$ centers with no ^{13}C near neighbors.)

For the second set of satellites, labeled y, the hyperfine interaction, within the accuracy and resolution of our measurements, was isotropic (see Table II). The anisotropy in the y satellite separation arising from the second-order $\underline{\mathbf{D}}$-matrix terms was greater than that from any anisotropy in the $\underline{\mathbf{A}}$ matrix.

B. Analysis of the temperature variation of the EPR spectrum

As the fine structure is small compared to the Zeeman interaction, we can (at least to a good approximation) use first-order perturbation theory to determine the parameters of the $\underline{\mathbf{D}}$ matrix as a function of temperature. We can easily derive equations for the splittings of the lines in the three principal crystallographic directions ($\langle 001\rangle$, $\langle 111\rangle$, and $\langle 110\rangle$). Working with the line splittings means that we can (to first order) ignore any temperature variation in the electronic $\underline{\mathbf{g}}$ matrix. In fact any variation proved too small to measure. Assuming that D_3 and D_2 lie in the $\{110\}$ symmetry plane of the defect, and θ is the angle that D_3 makes with [001], then we have three unknowns: D_3, D_1, and θ ($D_2=-D_1-D_3$). We have nine pieces of experimental data at each temperature: two for the Zeeman field along $\langle 001\rangle$, three for $\langle 111\rangle$ and four for $\langle 110\rangle$, corresponding to the measured $\underline{\mathbf{D}}$-matrix splittings. D_3, D_1, and θ were determined by allowing a least squares-fitting algorithm to vary these parameters until the best fit of nine derived equations with the experimentally measured splittings was obtained at each temperature. It was important to be careful about which transition on the high-field side is associated with which one on the low-field side. The $\underline{\mathbf{D}}$-matrix parameters are shown as a function of temperature in Fig. 5(a). The angle θ, which D_3 makes with [001] as a function of temperature, is shown in Fig. 5(b).

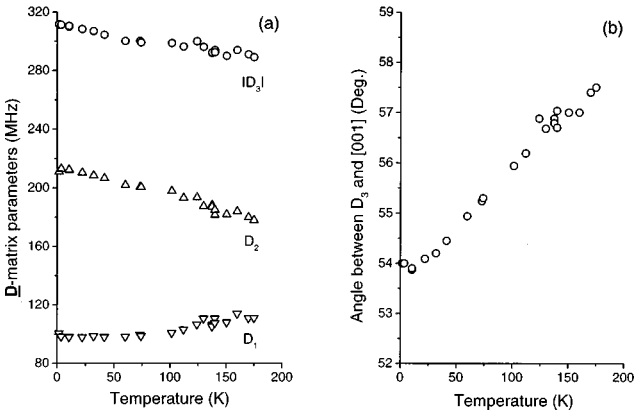

FIG. 5. (a) $\underline{\mathbf{D}}$-matrix parameters determined (using first-order perturbation theory), as a function of temperature. (b) Angle θ which D_3 makes with [001] in the (110) plane of the defect as a function of temperature. See text for more details.

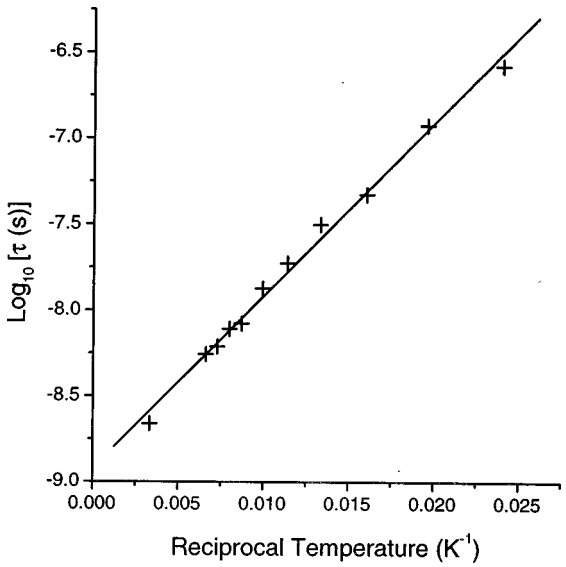

FIG. 6. The electron spin lifetime (in a given magnetic enviroment) deduced from the EPR linewidth in the usual way is plotted as a function of reciprocal temperature. For further details see text.

As can be seen from Fig. 3 it is not only the EPR line position that varies with temperature, above about 70 K the EPR linewidth broadens rapidly. At 300 K the linewidth is of order 2–3 mT. At first it was thought that the linewidth broadening resulted from thermally activated reorientation between different symmetry related sites. However, this is ruled out as the dominant mechanism for broadening as is explained in Sec. V E. In Fig. 6 the lifetime of the unpaired electron in a specific magnetic environment τ determined in the usual way from the linewidth broadening is plotted as a function of reciprocal temperature. The straight line in Fig. 6 is derived by assuming that the lifetime varies exponentially with reciprocal temperature. The activation energy determined from this fit was 20(1) meV.

V. DISCUSSION

We find in Sec. IV B that at low temperatures the *R*4/*W*6 defect has C_{2h} symmetry. In the following discussion we will refer to a specific site for which the plane of reflection symmetry is (110).

A. Analysis of the measured ^{13}C hyperfine interactions

In Sec. IV A it was shown that the *x* satellites arise from a ^{13}C atom in one of four equivalent positions, whereas the *y* satellites arise from a ^{13}C atom in one of two equivalent positions. The hyperfine parameters determined by fitting the experimental data to Eq. (2) are given in Table II. The ^{13}C hyperfine interaction determined from the *x* satellites is axially symmetric, and [for the site with the $(1\bar{1}0)$ plane of reflection symmetry] $A_{\|}$ is oriented (with equal probability) along one of the following four directions: [111],[$\bar{1}$11], [1$\bar{1}$1], or [11$\bar{1}$] (i.e., any ⟨111⟩ direction not in the plane of reflection symmetry).

The hyperfine interaction can be interpreted in the usual way in terms of an unpaired electron wave function

$$\Phi=\sum_i \eta_i(\alpha_i\phi_{2s}+\beta_i\phi_{2p}), \tag{3}$$

where the summation is over the carbon atoms on which the unpaired electron is localized and ϕ_{2s} and ϕ_{2p} are the $2s$ and $2p$ atomic orbitals, respectively. The parameters α_i, β_i, η_i, taken to be real, are deduced following the standard procedure from the hyperfine parameters and atomic parameters tabulated by Morton and Preston.[23] The hybridization ratio is $\lambda_i\equiv\beta_i/\alpha_i$. The wave-function parameters determined from the *x* ^{13}C hyperfine satellites are given in Table II. Eighty percent of the unpaired electron probability density is located on these four carbon atoms. The second, and smaller, interaction (corresponding to the two equivalent sites) was isotropic to within measurement and accounts for only a few percent of the unpaired electron probability density. Summing the fractional unpaired electron populations (η_i^2) determined from the measured hyperfine interactions shows that most of the unpaired electron probability density ($\sim$82%) is accounted for.

B. Possible models for *R*4/*W*6 indicated by the experimental evidence

In pure diamond *R*4/*W*6 is commonly formed in large abundance (Sec. III A) which makes it very likely that it has a simple structure. The center is formed at temperatures where vacancies are mobile. The correlation reported by Lea-Wilson *et al.*[8] between *R*4/*W*6 and the optical defect TH5, which is known to involve two vacancies, suggests a divacancy type of defect. The center contains an even number of electrons ($S=1$), and as it is produced in abundance in pure diamond with no dominant electron donors or acceptors we are forced to the conclusion that it is in the neutral charge state.

We find in Sec. IV B that at low temperatures the defect has C_{2h} symmetry. It is not clear from our measurements whether the symmetry of the center actually becomes D_{3d} at high temperatures, or that whether by chance $D_1=D_2$ (see Sec. V D).

The evidence suggests a simple structure involving two vacancies and C_{2h} symmetry implies that these, and any other constituents for the specific defect site being considered, lie in the (110) plane of reflection symmetry. The presence of the majority of the unpaired electron probability density on the four identical (symmetry related) carbon atoms implies either inversion symmetry for the defect, or reflection symmetry in the (110) plane. In either case, if there were other constituents, like interstitials, they would have to be present in equivalent pairs to preserve this symmetry. That implies too complex a structure for such an abundant center, so we are convinced that it comprises just two vacancies.

An undistorted [*V*-*C*-*V*] center would have reflection symmetry in the (110) plane, and is ruled out, as it would give the defect C_{2v} symmetry. Furthermore, the model is not consistent with the observed temperature variation of the EPR spectrum in particular the apparent ⟨111⟩ axial symmetry observed at 300 K.

The [*V*-*C*-*C*-*V*] center has the required C_{2h} symmetry. It is possible that a double bond would be formed between the

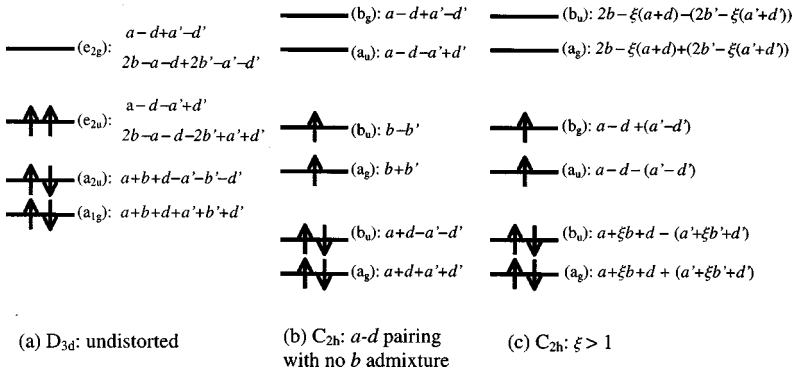

FIG. 7. Schematic diagram showing the different possible simple one-electron electronic structures of the ⟨111⟩ divacancy: (a) undistorted D_{3d} symmetry, (b) strong *pairing* distortion between a (a') and d (d') with no mixing between orbitals of the same symmetry, and (c) strong mixing of orbitals with the same symmetry with a_u and b_g shifted below the upper a_g and b_u orbitals. The labelling a, b, d, a', b', and d' of the dangling orbitals refers to Fig. 1. The arrows denote the electrons, and their spins, for the neutral charge state. See text for further details.

central two carbon atoms, as in acetylene. It then seems probable that a large fraction of the unpaired electron probability density would be found on the two remaining dangling orbitals in the (110) plane, at odds with the experimental findings. Even if the central carbon atoms were not so linked, it is improbable that the majority of the unpaired electron probability density would reside in four out of plane dangling bonds, coupled to form an $S=1$ state with equal probability density on each end, especially, when there is a full bonding orbital lying between them. Furthermore, we are unable to rationalize the model with the observed temperature variation of the EPR spectrum.

If the two vacancies were any further apart they would not perturb one another sufficiently for them to behave differently from two separated neutral vacancies with $S=0$ ground states.

The nearest-neighbor pair of vacancies $[V\text{-}V]^0$ is the only center that has not yet been ruled out. This defect must be distorted at low temperatures to account for the lowering of the expected symmetry to C_{2h}, and to give a large hyperfine interaction with four equivalent out-of-plane neighbors.

C. Accounting for the measured C^{13} hyperfine interactions with the $[V\text{-}V]^0$ model for $R4/W6$

In Sec. I B the electronic structure calculations on the $[V\text{-}V]^0$ center in diamond were reviewed. The simple defect molecule, with labeled dangling orbitals is shown in Fig. 1, and the one-electron energy levels in Fig. 7. A $^3A_{2g}$ ground state [originating from e_u^2 in Fig. 7(a)] was predicted for the undistorted $[V\text{-}V]^0$ center with D_{3d} symmetry and no Jahn-Teller distortion was expected.

We propose, at variance to previous theoretical predictions, that $[V\text{-}V]^0$ has C_{2h} symmetry at low temperature (the distortion is not Jahn-Teller in origin) and that the unpaired electron probability density is predominately localized in dangling orbitals on the four nearest-neighbor carbon atoms not located in the symmetry plane of the defect. As shown in Sec. V A about 80% of the unpaired electron probability density is accounted for on these four atoms. Further, we propose that the two equivalent carbon neighbors identified by the small isotropic ^{13}C hyperfine interaction are the two remaining in-plane nearest neighbors of the $[V\text{-}V]^0$ center. As we would expect for a vacancy center in diamond the majority of the unpaired electron probability density is localized on the carbon atoms adjacent the two vacancies. In the following sections, we show that all the as yet measured physical properties of $R4/W6$ can be explained in terms of the $[V\text{-}V]^0$ model.

Experience with the isolated vacancy in diamond has shown the importance of not ignoring the many electron effects for vacancy centers in diamond. However, to gain some insight into the problem we will proceed with the Watkins and Corbett model. Filling the levels of Fig. 7(b) (simplified pairing distortion ignoring the possible mixing between states of the same symmetry, i.e., the two a_g and two b_u states) with six electrons, indicates that we can make a $S=1$ state by filling the lowest a_g and b_u levels, and putting one electron in each of the higher a_g and b_u levels. This gives the localization of the unpaired electron on b and b' at odds with the experimental result. This problem is apparently solved if we allow the a_u and b_g levels to be shifted down in energy below the higher a_g and b_u levels. Now we have unpaired electron on the four out of plane dangling orbitals. However, this is implausible in the strong a-d pairing scheme because it would mean that dangling orbitals b and b' were totally unoccupied. However, if we switch to a scheme where two $a_g(b_u)$ levels are strongly admixed [Fig. 7(c)], then postulating a_u and b_g as the next lowest levels is not unreasonable. We can now have an $S=1$ state (one electron in each of the upper a_g and b_u levels) that would have the majority of the unpaired electron population density localized on a, d, a', and d', in accord with the experimental results. The filling of the one-electron levels described above indicates that the many electron ground state is ^3B_u. The simple one electron analysis given above is supported by recent work of Coomer *et al.*[24]

The hybridization ratio derived from the hyperfine interaction for carbon atoms a, d, a', and d' (Table II) suggests that these atoms move outwards (away from the vacancies) by ~ 0.02 nm. An outward displacement of a, d, a', and d', along with a much smaller outward or even inward (consistent with a small anisotropic hyperfine coupling) displace-

ment of b and b', is in accord with η of Fig. 7(c) being greater than 1 (strong mixing $\xi > 1$ and $l_{ad} > l_{ab} = l_{db}$). To the best of our knowledge, Coomer *et al.* were the first researchers to calculate this distortion for the $[V\text{-}V]^0$ center in diamond.[24] We note that this type of distortion has also been proposed for the $[V\text{-}V]^-$ in silicon,[16] and the As end of $[V\text{-}V]^{+,0,-}$ centers in GaAs.[25]

The experimental results can be rationalized in terms of the one electron model, but we would not want to over emphasize the one electron approach, a more sophisticated calculation is urgently required.

For $[V\text{-}V]^+$ in diamond we would expect a Jahn-Teller distortion to C_{2h} symmetry. However, we suggest caution in assuming that this would be a pairing distortion. When an e state splits under an e mode Jahn-Teller distortion, the two states split symmetrically and the total energy of the system is independent of the sign of the distortion. This leads to the Mexican-hat potential in e-mode space where the existence of a static distortion arises only from departures from linear Jahn-Teller coupling. The choice of the lowest energy static configuration and the height of the barrier for reorientation are determined by subtle higher order effects. This charge state of the divacancy in diamond should be sought and the sense of the distortion investigated.

We have to ask ourselves what drives the distortion for the $[V\text{-}V]^0$ center in diamond? We believe that the distortion is not Jahn-Teller in origin ($^3A_{2g}$ ground state predicted for D_{3d} symmetry). The increase in strain energy associated with the distortion must be compensated for by a greater reduction in the total electronic energy. The large open volume of the divacancy suggests that lattice relaxation will be at least as important as for the isolated vacancy. Our results show that the lattice relaxation around the V^0, V^-, and $[V\text{-}V]^0$ centers in diamond, is outwards and has similar magnitude in all three cases. We hope that this work stimulates theoretical investigation.

D. The origin and temperature variation of the $\underline{\mathbf{D}}$ matrix

Low-temperature EPR measurements (Sec. III C) show that the $R4/W6$ center has a spin-triplet state ($S=1$) ground state and the largest component of the $\underline{\mathbf{D}}$ matrix (D_3) is negative. The final piece of information is consistent with the $\underline{\mathbf{D}}$ matrix arising from a dipole-dipole interaction between two unpaired electrons with $S=\frac{1}{2}$. If we assume that the magnitude of D_3 originates solely from a dipole-dipole interaction between two electrons, then this suggests an electron-electron separation of the order of 0.6 nm. At such a large separation one would expect the $\underline{\mathbf{D}}$ matrix to be axially symmetric, which is far from so for $R4/W6$ (see Table I). Hence, the data is not consistent with the $\underline{\mathbf{D}}$ matrix originating from two well-separated unpaired electrons.

The $[V\text{-}V]^0$ model described in Sec. V C indicates that the unpaired electron probability density is primarily localized on two pairs of carbon atoms a', d' and a and d. These pairs of atoms are separated from one another by about 0.3 nm, so if one attempted to preserve the explanation of $\underline{\mathbf{D}}$ arising purely from a dipole-dipole interaction, the value of D_3 would be ~ -1640 MHz, even after allowing for the 80% spin occupancy of the orbitals. To make a correct estimate of $\underline{\mathbf{D}}$ one would need to sum the dipole-dipole interaction over the distributed orbitals. This would undoubtedly lead to far from axial symmetry, as is observed, but would predict values considerably larger than the measured interaction.

This analysis need not invalidate the nearest-neighbor divacancy model, because there may be other contributions to the $\underline{\mathbf{D}}$ matrix. The shift of g value from the free-spin value g_e for $R4/W6$ (Table I) is large compared with most defects in diamond,[26] and it arises from a spin-orbit admixture of excited states. In a free atom such admixtures also lead to a contribution to the $\underline{\mathbf{D}}$ matrix of the form $\underline{\mathbf{D}} = \lambda_{SO}\delta\mathbf{g}/g_e$, where λ_{SO} is the spin-orbit coupling constant. If such a mechanism produced a contribution to $\underline{\mathbf{D}}$ in $R4/W6$, the sign and magnitude could be such that it opposes and almost cancels the dipole-dipole contribution. Unfortunately, for a distributed wave function, a calculation of all these effects is far from straightforward, so these considerations only give an indication of how the measured $\underline{\mathbf{D}}$ matrix may be reconciled with the model.

In Sec. III D is was shown that the magnitude of the $\underline{\mathbf{D}}$ matrix decreased with increasing temperature. Any dipole-dipole contribution to $\underline{\mathbf{D}}$ would decrease in magnitude as the temperature increased, as is observed. If the whole of the observed $\underline{\mathbf{D}}$ were attributed to dipole-dipole interaction any change in D_3 due to a lattice contraction would be at least a factor of five smaller than what we observe. However, if 80% of the dipole-dipole interaction were cancelled by the other mechanisms mentioned above, the observed temperature variation could be accounted for by the effect of thermal expansion of the dipolar contribution. However, this would involve making the unlikely assumption that the other contributions to the $\underline{\mathbf{D}}$ matrix are independent of lattice contraction. In addition, the measured change is linear over the entire temperature range, while there is considerable curvature in the dependence of a_0 upon temperature.[27] The apparent rotation of the $\underline{\mathbf{D}}$ matrix might result from different dependencies of the two competing mechanisms.

This sort of temperature dependence of the $\underline{\mathbf{D}}$ matrix is unusual in diamond. Kim *et al.*[28] reported that for the defect labeled $A2$, created after electron or neutron irradiation, the $\underline{\mathbf{D}}$ matrix parameters increased and rotated about the axis perpendicular to the symmetry plane of the defect as the temperature is increased from 77 to 300 K.[28] Further study is required to develop a good understanding of the temperature variation of the $\underline{\mathbf{D}}$ matrix for $R4/W6$ and $A2$.

E. The temperature variation of the EPR linewidth

For each possible orientation of the $\langle 111 \rangle$ divacancy (Fig. 1) there are three entirely equivalent possible distortions. In each case one of the nearest-neighbor separations (l_{ad}, l_{ab}, or l_{bd}) is unique while the other two are equal. The barrier to reorientation from one distortion to another should not be large and we expect thermally activated reorientation to manifest itself at relatively low temperatures. Indeed for the positively and negatively charged $\langle 111 \rangle$ divacancies in silicon the activation energy is only 73(2) and 56(2) meV, respectively, and lifetime broadening is observed at temperatures above about 50 K. At first sight the linewidth broadening observed for the $\langle 111 \rangle$ divacancy in diamond invites this interpretation, however, this is not the correct explanation.

The outermost transitions shown in Fig. 3 should not be broadened by reorientation between differently distorted configurations because the resonance field is identical for each of the three differently distorted sites. These transitions are clearly broadened as the temperature increases, ruling out thermally activated reorientation between different distortions as the dominant mechanism for line broadening.

Analysis of the linewidth broadening in Fig. 6 indicated an activation energy for lifetime broadening of 20(1) meV with a pre-exponential factor $1/\tau_0 \approx 10^9\ \mathrm{s}^{-1}$. The activation energy for lifetime broadening is not unreasonable for a energy barrier to reorientation, however the prefactor is 3 to 4 orders of magnitude smaller than expected for reorientation between different distortions.

We propose that the EPR line broadening originates from rapid spin-lattice relaxation at high temperatures. In diamond, with the exception of transition metal ion centers, spin-lattice relaxation times (T_1) are typically very long, and EPR spectra are easily saturated. This suggests that the dominant spin-lattice relaxation mechanism is direct relaxation, which involves direct nonradiative transitions between the spin levels. At low temperatures (below 50 K) the $R4/W6$ EPR spectrum is easily saturated and the EPR residual linewidth is determined by unresolved hyperfine structure and electron spin-spin broadening. However, as the temperature is increased and the EPR lines broaden the transitions become increasingly more difficult to saturate. A rapid reduction in T_1 with increasing temperature requires more efficient spin lattice-relaxation, this is possible via the Orbach mechanism. The Orbach process involves an excited state at an energy Δ above the ground state, where Δ is less than the maximum phonon energy. A transition between the one of the M_S levels in the ground state and excited state can be driven by the direct absorption of a phonon of the appropriate energy. The reverse transition can occur by the emission of a phonon of a slightly different energy resulting in population of a different M_S level in the ground state. This indirect transfer of population between the different M_S levels of the ground state can constitute very effective spin-lattice relaxation. It can be shown that when Orbach relaxation dominates $1/T_1$ varies as $\exp(-\Delta/k_B T)$ when $\Delta \geqslant k_B T$.[29]

The observed exponential dependence of the lifetime broadening of the EPR transitions with reciprocal temperature (Fig. 6) is entirely consistent with rapid spin-lattice relaxation via the Orbach mechanism above 50 K. Further, this result indicates that there is a low-lying state, approximately 20 meV above the ground state. The existence of this state is not inconsistent with our EPR intensity measurements. We have not been able to make EPR measurements at high enough temperatures to measure a thermal depopulation of the ground state. The magniture of the pre-exponential factor $1/\tau_0 \approx 10^9\ \mathrm{s}^{-1}$ is consistent with that we would expect for Orbach relaxation.[29]

VI. CONCLUSIONS

We conclude that the EPR evidence is consistent only with the $R4/W6$ EPR center being two nearest-neighbor vacancies in the neutral charge state ($[V\text{-}V]^0$). The defect is formed in abundance when the vacancy becomes mobile at ~ 900 K, such that nearly all the vacancies are lost while the $R4/W6$ center is formed in pure diamond. At low temperatures the $[V\text{-}V]^0$ center has C_{2h} symmetry, which is surprising in light of theoretical predictions. Analysis of the ^{13}C hyperfine interactions indicates that at low temperature $\sim 80\%$ of the unpaired electron probability density is located in dangling orbitals on four equivalent carbon atoms not in the $(1\bar{1}0)$ symmetry plane of the defect. A smaller, isotropic ^{13}C hyperfine interaction indicates two more equivalent carbon neighbors. They are interpreted as being the remaining two (in-plane) nearest neighbors. The nature of the localization of the unpaired electron probability density is radically different for $[V\text{-}V]^0$ in diamond from $[V\text{-}V]^+$ and $[V\text{-}V]^-$ in silicon. The temperature dependent EPR linewidth in the temperature range 50–300 K is attributed to rapid spin lattice relaxation via the Orbach process. This interpretation suggests the existence of excited state about 20 meV above the ground state. A direct measurement of the temperature dependence of the spin lattice relaxation rate would be useful to confirm this interpretation. The symmetry of the **g** matrix and **D** matrix are consistent with the symmetry of the model. However, a detailed interpretation of the magnitudes of these parameters has not yet been attempted. The temperature variation of the **D** matrix is intriguing and deserves further study.

Although the nearest-neighbor divacancy in diamond has been identified, many questions remain; particularily, what is the explanation of the driving force for the distortion to C_{2h} symmetry. It would be very interesting to investigate the symmetry lowering distortion by stress induced alignment. In addition, stress induced alignment of the axis of the divacancy as it is formed would be interesting. We have no measurement of the energy required for reorientation of the divacancy axis. In silicon it has been shown that the divacancy migrates as a unit without dissociating; and the divacancy is reorienting as it diffuses, so the binding energy must be greater than the reorientation energy. Perhaps in diamond the divacancy dissociates before reorienting. Further investigation is required to answer these questions.

ACKNOWLEDGMENTS

This work was supported by the Engineering and Physical Sciences Research Council (EPSRC) Grant No. GR/L65772. D.J.T. thanks Merton College, Oxford, and De Beers Industrial Diamond Division for financial support. M.E.N. acknowledges EPSRC for support. We would like to thank B. J. Coomer, J. P. Goss, R. Jones, G. D. Watkins, and G. Davies for technical advice.

*Author to whom correspondence should be addressed.

[1] C.A. Coulson and M.J. Keresley, Proc. R. Soc. London, Ser. A **241**, 433 (1957).

[2] M. Lanoo and A.M. Stoneham, J. Phys. Chem. Solids **29**, 1987 (1968).

[3] J. Isoya, H. Kanda, Y. Uchida, S. C. Lawson, S. Yamasaki, H. Itoh, and Y. Morita, Phys. Rev. B **45**, 1436 (1992).

[4] J.A. van Wyk, O.D. Tucker, M.E. Newton, J.M. Baker, G.S. Woods, and P. Spear, Phys. Rev. B **52**, 12 657 (1995).

[5] D.P. Joubert, Lin Li, and J.E. Lowther, Solid State Commun. **100**, 561 (1996).

[6] S.J. Breuer and P.R. Briddon, Phys. Rev. B **51**, 6984 (1995).
[7] G. Davies, S. C. Lawson, A. T. Collins, Alison Mainwood, and Sarah J. Sharp, Phys. Rev. B **46**, 13 157 (1992).
[8] M.A. Lea-Wilson, J.N. Lomer, and J.A. van Wyk, Philos. Mag. B **72**, 81 (1995).
[9] C.D. Clark, R.W. Ditchburn, and H.B. Dyer, Proc. R. Soc. London, Ser. A **237**, 75 (1956).
[10] C.A. Coulson and F.P. Larkins, J. Phys. Chem. Solids **30**, 1963 (1969).
[11] Lin hong Li and J.E. Lowther, Phys. Rev. B **53**, 11 277 (1996).
[12] G.D. Watkins, in *Defects and Their Structure in Non-Metallic Solids*, edited by B. Henderson and A.E. Hughes (Plenum, New York, 1976).
[13] F.G. Anderson, F.S. Ham, and G. Grossmann, Phys. Rev. B **53**, 7205 (1996).
[14] H. Seong amd L.J. Lewis, Phys. Rev. B **53**, 9791 (1996).
[15] G.D. Watkins and J.W. Corbett, Phys. Rev. **138**, A543 (1965).
[16] M. Saito and A. Oshiyama, Phys. Rev. Lett. **73**, 866 (1994).
[17] G.D. Watkins, Phys. Rev. Lett. **74**, 4353 (1995).
[18] M. Saito and A. Oshiyama, Phys. Rev. Lett. **74**, 4354 (1995).
[19] D.J. Twitchen, M.E. Newton, J.M. Baker, O.D. Tucker, T.R. Anthony, and W.F. Banholzer, Phys. Rev. B **54**, 6988 (1996).
[20] W.V. Smith, P.P. Sorokin, and G.J. Lasher, Phys. Rev. **115**, 1546 (1959).
[21] D.J Twitchen, D.C. Hunt, V. Smart, M.E. Newton, and J.M. Baker, Diamond Relat. Mater (to be published).
[22] A.T. Collins and W.S. Williams, J. Phys. C **4**, 1789 (1971).
[23] J. Morton and K. Preston, J. Magn. Reson. **30**, 577 (1978).
[24] B.J. Coomer, J.P. Goss, R. Jones, S. Öberg, and P.R. Briddon (private communication) .
[25] S. Pöykkö, M.J. Puska, and R.M. Nieminen, Phys. Rev. B **53**, 3813 (1996).
[26] C.A.J. Ammerlaan, in *Landolt-Bornstein Numerical Data and Functional Relationships in Science and Technology*, edited by O. Madelung and M. Schultz, New Series Group III, Vol. 22, pt. b (Springer, Berlin, 1990), p. 117.
[27] J. Thewlis and A.R. Davey, Philos. Mag. **7**, 409 (1956).
[28] Y.M. Kim, Y.H. Lee, P. Brosious, and J.W. Corbett, *Defects in Semiconductors* (Institute of Physics, London, 1972), Vol. 4, P. 202.
[29] A. Abragam and B. Bleaney, *Electron Paramagnetic Resonance of Transition Ions* (Dover, New York, 1986).